

Electron-Atom (Molecule) Collision Processes

Sandor Trajmar

Electron-atom (molecule) collision physics is concerned with the many processes that can take place as the result of such collisions. These are of interest for a variety of reasons, ranging from understanding the fundamental nature of the interactions to quantitatively determining the probabilities associated with various processes and applying the data on collisions to understand the behavior of practical systems in which they play an important role.

The initial studies of electron-atom (molecule) collision phenomena in the 1930's significantly contributed to our understanding of the structure and quantum states of matter. After a few decades of dormancy, the field has experienced a renaissance since the late 1950's. This has been due, in part, to advances in vacuum techniques, charged and neutral particle beam technology, electron energy analysis and detection, and computer science; it is also partly due to the need for electron collision data in connection with plasma and laser systems, ionospheric phenomena, and so on. At the same time, a great deal of progress has been made in the theoretical area, and the interplay between theory and experiments has further enhanced developments in this field.

It is not possible to cover all present-day activities in a short article. I will confine my discussion to electron collisions with gaseous atomic and molecular species at low and intermediate energies (from near threshold to a few hundred electron volts). Under these conditions, elastic and superelastic scattering, excitation (rotational, vibrational, and elec-

tronic), ionization, dissociation, electron capture, and their various combinations represent the most important processes. I will give a brief introductory background and discuss several processes in connection with illustrative examples. The presentation will be from the experimental point of view, and theory will be discussed only as needed to interpret the experimental observations. The spectro-

Summary. Electron-atom (molecule) collision processes at low and intermediate energies are discussed. Measurements of collision cross sections are described briefly. The experimental techniques and the interpretation of observations are illustrated by specific examples.

scopic aspects of electron impact measurements have been reviewed by several authors in recent years. A short discussion on this subject and references are given by Trajmar (1). For a more detailed treatment of the whole area of electron collision phenomena, the reader is referred to the monographs of Massey and Burhop (2).

Experimental Techniques and Procedures

To obtain cross sections from measurements carried out under multiple-collision conditions (swarm technique), the solution of the Boltzmann equation, which contains the cross sections as parameters, is required. Although these types of investigations yield reliable momentum transfer and integral excitation cross sections at low impact energies (up to a few electron volts), they become

ambiguous at higher energies and cannot yield differential cross-section data.

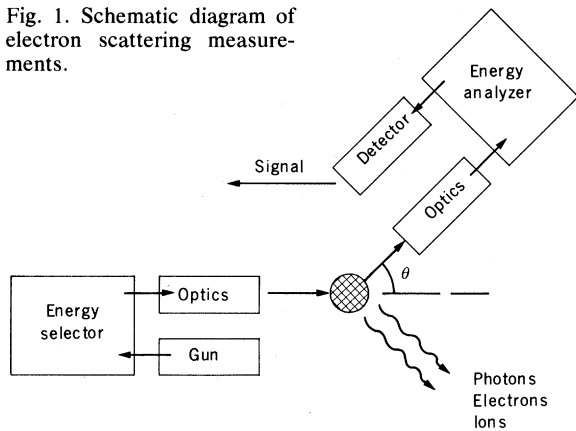
Interpretation of electron scattering results is easiest and most unambiguous when the measurements are carried out under single-collision conditions (the electron mean free path is large compared to the target size). Both static and beam targets have been utilized for this type of experiment, but the latter are more suitable for quantitative measurements of differential cross sections and are most frequently used. In this article I consider beam-beam scattering experiments that are conceptually simple: A nearly monoenergetic electron beam is scattered by a target atomic beam and the energy and angular distribution of the scattered electrons are measured. In practice, however, one encounters a number of difficulties, and usually a compromise is needed between a number of contradicting requirements.

A schematic diagram of an electron scattering arrangement is shown in Fig. 1. Electrons are extracted from a therm-

ionic source and collimated in the gun. The energy selector extracts electrons with a narrow energy distribution from this beam, which is then focused onto the target beam with the required impact energy (E_0). Electrons scattered through the polar angles θ and ϕ with respect to the original beam are collected over a small solid angle ($\sim 10^{-3}$ steradian), energy-analyzed, and recorded as a function of some parameter by pulse counting and multichannel scaling techniques. During the collision other, secondary particles (electrons, photons, ions) can also be generated and detected, either individually or in various combinations of coincidences. The electron optics consist of combinations of apertures or cylinder lenses (or both) having achromatic or other desired characteristics. The en-

The author is head of the Electron Collision Processes Group at Jet Propulsion Laboratory, California Institute of Technology, Pasadena 91103.

Fig. 1. Schematic diagram of electron scattering measurements.



energy selector and analyzer are usually cylinders or hemispheres in which electrostatic deflection is used to spatially separate electrons with different energies, although other types of energy selectors, such as retarding field analyzers, trochoidal monochromators, Wien filters, and Mollenstadt analyzers, have also been used with success. The target beam is generated by effusing a gas through an orifice, tube, or capillary array with or without further collimation.

Supersonic nozzle beams have frequently been used to achieve high target densities and high-temperature crucible sources for materials with a low vapor pressure at room temperature. The experiments are carried out in a vacuum chamber ($\sim 10^{-6}$ torr background pressure) and special care must be exercised to eliminate the effects of electric and magnetic fields.

The scattering apparatus can be operated in a number of ways. Most commonly,

the intensity of the scattered electron signal is measured as a function of energy loss (ΔE) at a fixed impact energy (E_0) and scattering angle (θ). (We assume here that the scattering is independent of the azimuthal angle, ϕ .) An example of the resulting energy-loss spectrum for He in the range 19.5 to 25.5 eV is shown in Fig. 2 (3). The zero energy-loss feature (not shown) corresponds to elastic scattering. (Superelastic scattering would appear on the left side of

the elastic peak.) The features shown in Fig. 2 correspond to excitation of various electronic states. An energy-loss spectrum can also be generated by the constant residual energy mode. In this case the analyzer is tuned to transmit electrons that have a specific residual energy (E_R) after the scattering process. That is, the condition $E_R = \text{constant} = E_0 - \Delta E$ is satisfied during the scanning of the energy-loss spectrum (at a fixed scattering angle). In the spectrum, then, each feature or transition is generated at the same impact energy above its own threshold. This mode of operation is useful in near-threshold experiments, where the energy sensitivity of the detector optics could drastically alter the energy-loss spectrum if the first method was used. An example for this mode is shown in Fig. 3 (4). In the third method of operation, the detector is set to transmit only signals corresponding to a specific energy-loss channel (ΔE and θ fixed) as a function of impact energy. This method is used to study resonances and cusps that appear in the various energy-loss channels. See Fig. 4 (5) for an example.

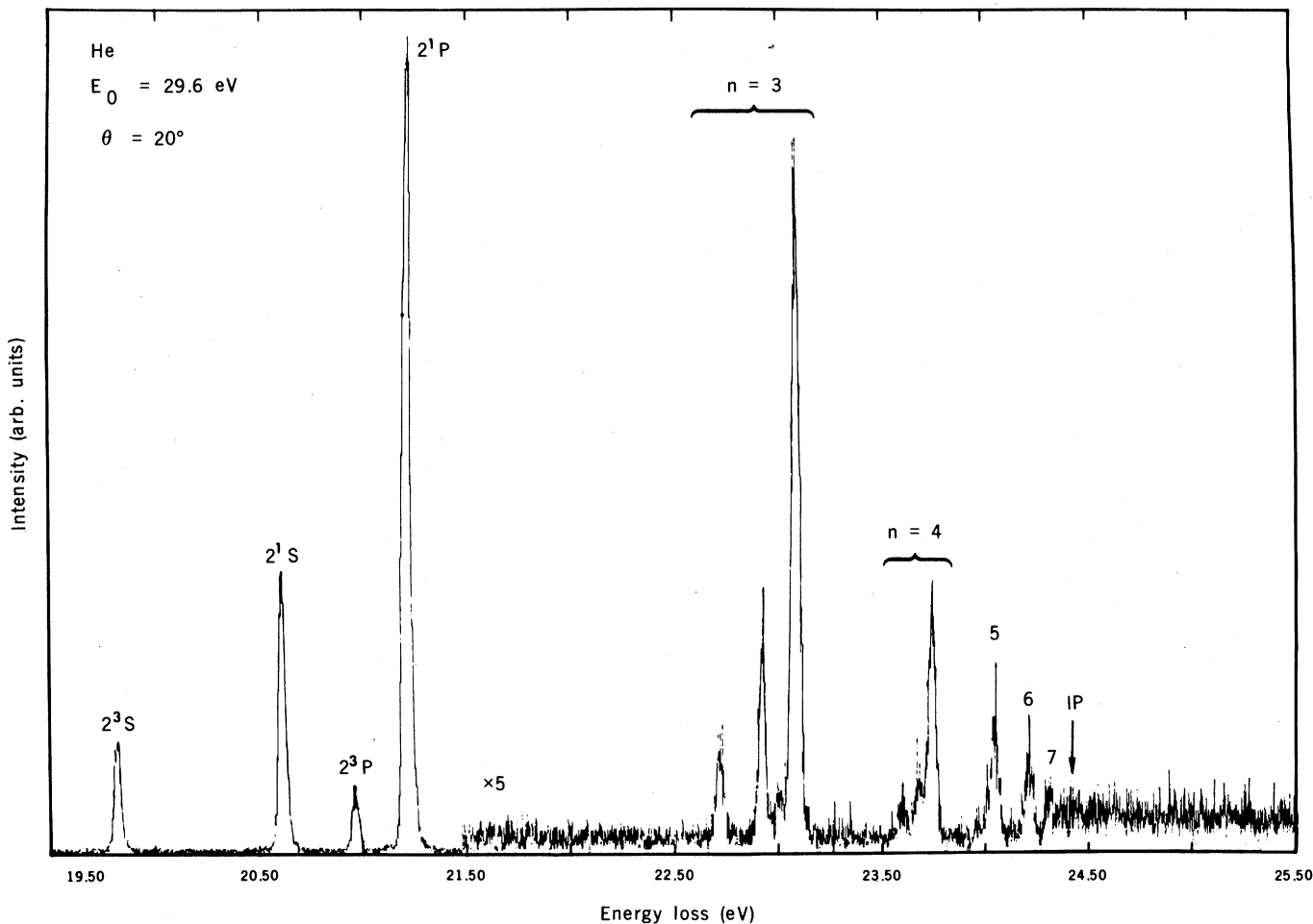


Fig. 2. Energy-loss spectrum of He at impact energy 29.6 eV and scattering angle 20° . The principal quantum numbers and spectroscopic symbols for the excited states are indicated; *IP*, ionization potential.

Electron Impact Cross Sections

The quantity that characterizes a scattering process is known as the cross section, σ . It represents the (time-independent) probability of occurrence of a particular event. The idea of a unique collision diameter is not applicable to electron collisions. Because of the long-range nature of the electron-molecule interaction potential, the distance for an effective interaction depends strongly on electron velocity and it is more useful to define energy-dependent cross sections. In experiments where the scattered electrons are detected as a function of impact energy, scattering angle, and energy loss, we define the triply differential cross section as $\partial^3\sigma/\partial E_0\partial\Omega\partial E$, where Ω stands for θ and ϕ . For studies of discrete excitation processes, this quantity is usually integrated over the line profile to give the doubly differential cross section $[\partial^2\sigma/\partial E_0\partial\Omega]_n$ for transition n . At impact energies away from resonances, the cross section changes slowly with impact energy and can be considered constant over the finite impact-energy distribution. Therefore it is only necessary to define the singly differential cross section $[\partial\sigma/\partial\Omega]_n$. In conventional electron experiments (target molecules randomly oriented), the scattering is independent of ϕ and depends only on θ . We then define the differential cross section as $[\partial\sigma/\partial\theta]_n \equiv \text{DCS}_n$. Integration over all scattering angles yields the integral and momentum transfer cross sections for process n as

$$Q_n(E_0) = 2\pi \int_0^\pi \text{DCS}_n(E_0, \theta) \sin\theta d\theta \quad (1)$$

$$Q_n^M(E_0) = 2\pi \int_0^\pi \text{DCS}_n(E_0, \theta) \times \left[1 - \frac{k_n}{k_0} \cos\theta \right] \sin\theta d\theta \quad (2)$$

where k_0 and k_n are the magnitudes of the initial and final momenta of the electron, respectively. The integral cross sections are the quantities required in many practical applications, and they can also be measured directly. However, differential cross sections are needed to obtain momentum transfer cross sections, detailed information about the nature of electron-target interactions, and properties of the target, as well as to make strict checks of theoretical models. Total scattering cross sections representing the sum of all integral cross sections ($Q_{\text{TOT}} = \sum_n Q_n$) can also be measured experimentally by electron transmission or target recoil techniques, but they give even less information about the details of scattering processes than integral cross sections.

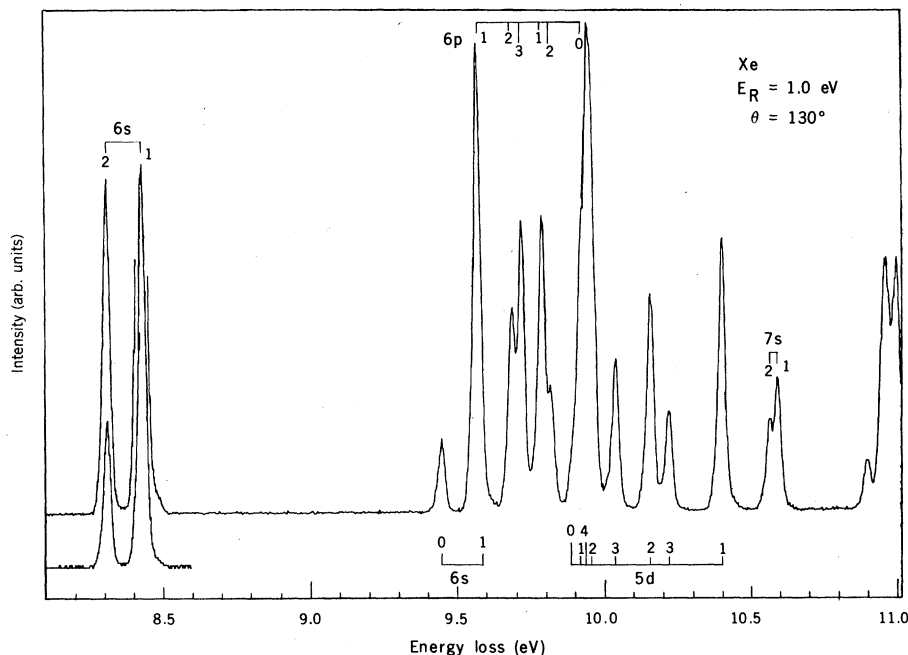


Fig. 3. Energy-loss spectrum of Xe obtained at the constant residual energy of 1 eV and a 130° scattering angle. The excited electron orbitals and J values are given for all transitions.

In experiments where the electron signal is measured concurrently with some other secondary particle (photon, electron, or ion), higher order differential cross sections (with respect to the energy and scattering angle of the second particle) can be defined and measured.

Differential cross sections are related to measured scattering intensities in a rather complicated way, and their accurate measurement (within a few percent) is still a difficult problem in electron scattering at low and intermediate energies. The relationship is

$$I_n(E_0, \theta) = F(E_0) \overline{\text{DCS}}_n(E_0, \theta) \times \int_V \int_{\Omega(\mathbf{r})} \rho_N(\mathbf{r}) f_e(\mathbf{r}) d\Omega d\mathbf{r} \quad (3)$$

where I is the scattering intensity, F is the overall instrument efficiency factor, $\overline{\text{DCS}}(E_0, \theta)$ is the value of the differential cross section at the nominal values of E_0 and θ averaged over the energy and an-

gular resolution of the apparatus, $\rho_N(\mathbf{r})$ and $f_e(\mathbf{r})$ are the spatial distribution of target density and electron beam flux in the scattering volume V seen by the detector. In the straightforward method of determining cross sections it is necessary to know $F(E_0)$ and the integral, which is called the effective path length or effective scattering volume.

The experimental procedure for obtaining accurate (~ 5 to 10 percent) cross sections at low and intermediate electron energies is difficult and tedious. The availability of such cross sections is limited mainly for this reason. In recent years, elastic cross sections for helium have been determined with high accuracy (6) and they can be used in relative measurement procedures (7) as a calibration standard for other species. This method is expected to generate accurate cross sections for a large body of electron scattering processes.

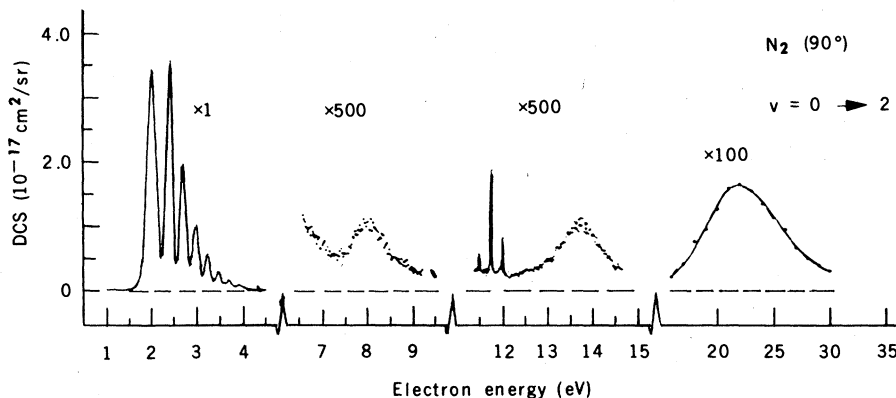


Fig. 4. Resonances in the vibrational excitation channel of N_2 at a 90° scattering angle.

From the theoretical point of view, the cross section is proportional to the square of the scattering amplitude, which is defined in terms of the transition matrix elements

$$\text{DCS}_n \propto |f_n|^2 \propto |\langle \psi_n | T | \psi_0 \rangle|^2 \quad (4)$$

where f_n is the complex scattering amplitude, T is the transition operator, and ψ_0 and ψ_n are the wave functions describing the system (including the scattering electron) in the initial and final states, respectively. The theoretical efforts are concerned with finding reasonable approximations to the wave functions and transition operators.

Electron-Atom (Molecule) Collision Processes

For the purpose of discussion, it is convenient to divide electron collision processes into low-, intermediate-, and high-energy regions, with impact energies ranging from threshold to a few electron volts, from a few to a few hundred

electron volts, and from a few hundred to a few thousand electron volts, respectively. Here I will emphasize the regions of low and intermediate energy and treat high-energy scattering only briefly.

Low-Energy Collisions—Resonances

Electron impact energy-loss spectra obtained at low impact energies (and high scattering angles) are frequently dominated by optically forbidden excitations. Processes requiring spin change are especially easily achieved at these energies by electron exchange. This effectiveness of low-energy electrons in generating metastable species is utilized in electric discharge devices and can also be used to gain spectroscopic information that is not obtainable by conventional optical spectroscopy. Specific examples of this application of low-energy electrons will be discussed to some extent in the section on electron impact processes.

Another characteristic of low-energy

scattering is that the electron impact cross sections are frequently dominated by resonances and change drastically with impact energy. The velocity of the incoming electron at these energies is comparable to the velocities of the outer valence electrons of the atom or molecule, and it is appropriate to treat the incident electron as if it were temporarily attached, giving rise to a negative atomic or molecular ion. The negative ion state exists for a time longer than the orbital period and it has identifiable properties. Although the concept of compound state formation has been widely utilized in nuclear physics, it was discovered in electron scattering only about 15 years ago (8) and became the subject of extensive studies only recently (9).

Resonances are usually classified as either closed- or open-channel resonances depending on whether they lie energetically below or above the state from which they derive (parent state). In the first case, the interaction between the target and the incoming electron results in excitation of the target. This, in turn, creates a well sufficiently deep to capture the electron for a short time. This type of resonance is usually called a Feshbach resonance; it appears just below some excited (parent) state, has a relatively long lifetime, and decays into all underlying states. Open-channel resonances or shape resonances are also created by distortion of the target. The electron in this case is captured by the angular momentum barrier of a well created by the influence of the incoming electron. These resonances lie above the parent state and decay predominantly into the parent state.

The interference between direct and resonant scattering determines the line shape of resonance features. The cross section in the resonance region is described by the formula of Fano and Cooper (10)

$$\sigma(E) = \sigma_r \left[\frac{(q + \epsilon)^2}{1 + \epsilon^2} \right] + \sigma_b \quad (5)$$

Here σ_r and σ_b are the resonant and non-resonant (background) parts of the cross section, q is the line profile index, and $\epsilon = 2(E_0 - E_r)/\Gamma$, where Γ is the resonance width and E_r the resonance energy.

A global view of resonances is shown in Fig. 4 for N_2 in the decay channel corresponding to vibrational excitation of the molecule (5). Four distinct types of resonances appear. Between 1 and 4 eV the structure is due to a ground-state shape resonance. The lifetime of the resonant state is comparable to the vibrational time of the molecule ($\sim 10^{-14}$ second) and the structure is caused by an

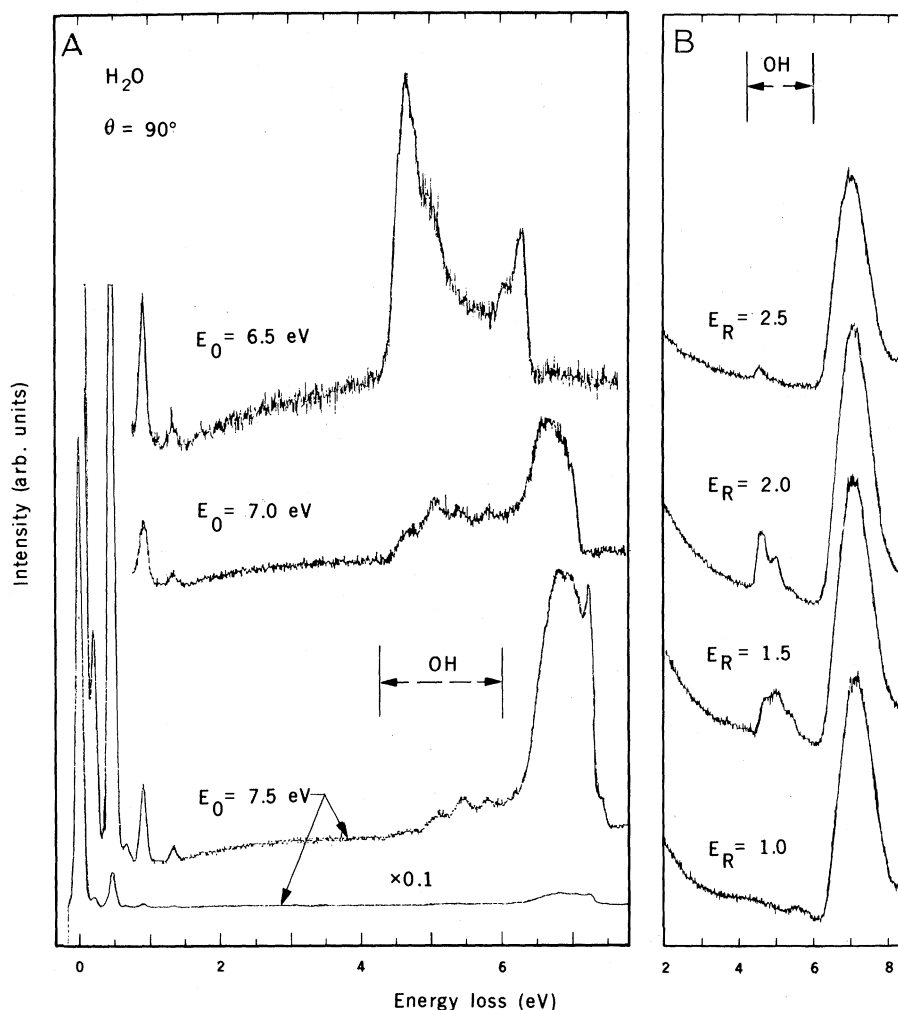


Fig. 5. Energy-loss spectra of H_2O obtained (A) at constant electron impact energies of 6.5, 7.0, and 7.5 eV and (B) at four constant residual energies. The regions marked by OH represent vibrational excitation of OH and the signal there corresponds to H^- instead of scattered electrons.

interference effect in the nuclear wave function. In the regions 7 to 9 eV and 12 to 15 eV the broad shape resonances are associated with excited N_2 states (lifetime short compared to the vibrational period). The sharp peaks in the region 11 to 12 eV are caused by long-lived Feschbach-type (closed-channel) resonances. Finally, the very broad resonance between 15 and 30 eV is also associated with shape resonances with very short lifetimes.

Resonant electron capture by molecules and subsequent dissociation of the molecules into neutral or ionic species have been the subject of extensive studies in recent years (11). If the resonance state is formed on the repulsive part of its potential energy curve and is above its dissociation limit, the nuclei start to separate, gain kinetic energy, and dissociation takes place. If one atom (or fragment) has a positive electron affinity, a stable negative ion fragment will be formed (dissociative attachment), otherwise the products will be neutral fragments plus an electron. An example of this process is shown in Fig. 5 for H_2O (12). The process is $H_2O + e^- (\sim 6.5 \text{ eV}) \rightarrow H_2O^- \rightarrow H^- + OH(\nu, J)$. The H^- ion is detected in the electron (e^-) energy-loss spectrum with electrostatic spectrometers and its energy and angular distributions can be determined. In Fig. 5 the H^- energy distribution is represented by the structure at an energy loss of around 4.5 eV. (The other structures are due to electrons and can be eliminated from the spectrum by applying a magnetic field in front of the detector.) The structure in the energy distribution of H^- corresponds to OH being produced in various vibrational states (ν). The increased width of the vibrational transitions (compared to electron elastic scattering) indicates that the OH fragment is excited rotationally also (J).

The resonant state has a finite lifetime and may decay to some excited neutral molecular state before dissociation can take place. In Fig. 6 this decay leads to vibrational excitation of the ground electronic state of the NO molecule (13). By this procedure highly vibrationally excited NO is produced, since the decay can take place over the whole potential energy curve.

The large, resonance-dominated cross sections for vibrational and rotational excitations are important in plasma and gas laser systems. One of the most efficient lasers, the N_2 - CO_2 laser, relies on efficient vibrational excitation of N_2 in the energy region 1 to 4 eV (and on subsequent transfer of this vibrational energy to the CO_2 molecule). Resonances associated with electronic excitations

have, in general, a much smaller effect on the cross sections.

Studies of angular distributions associated with resonances in elastic and various inelastic channels give information concerning the character of the negative ion state. Very frequently, however, the resonances are detected in the total electron scattering cross section (by electron transmission or target recoil measurements) or in optical excitation functions.

Electron Impact Excitation at High Energies

Electron impact processes at high impact energies have been extensively studied. Excitation of valence shell electrons as well as intermediate and inner shell excitations have been investigated, and a great deal of work aimed at obtaining charge densities and momentum densities in atoms and molecules has also

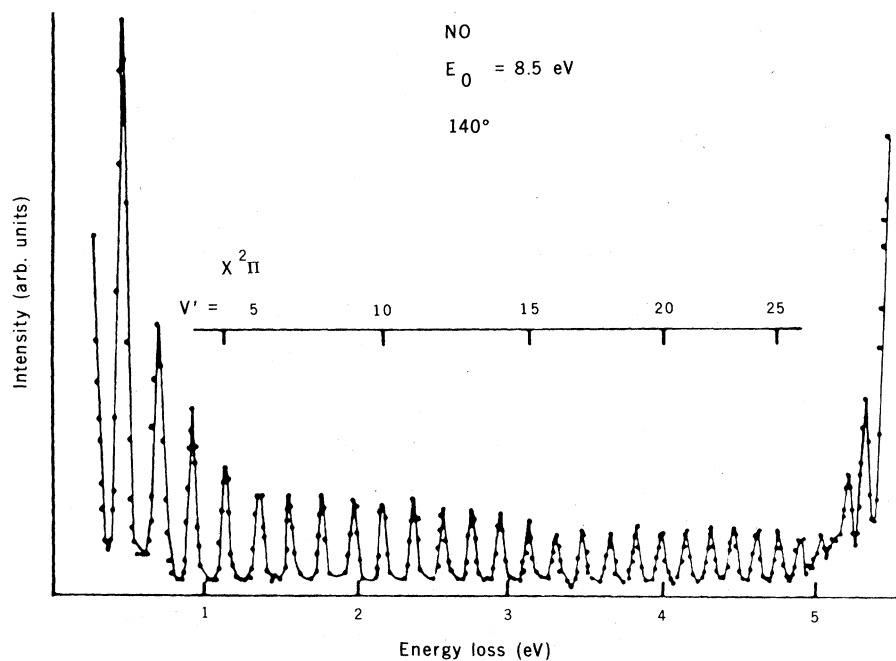


Fig. 6. Energy-loss spectrum of NO. The vibrational quantum numbers (ground electronic state) are indicated.

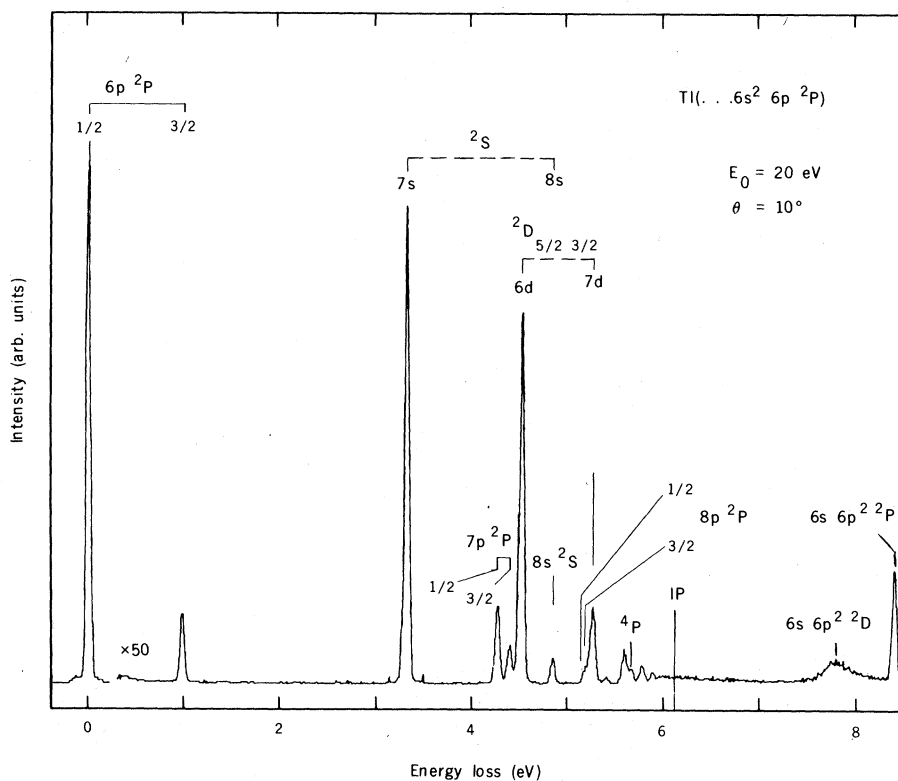


Fig. 7. Energy-loss spectrum of TI below the first ionization limit.

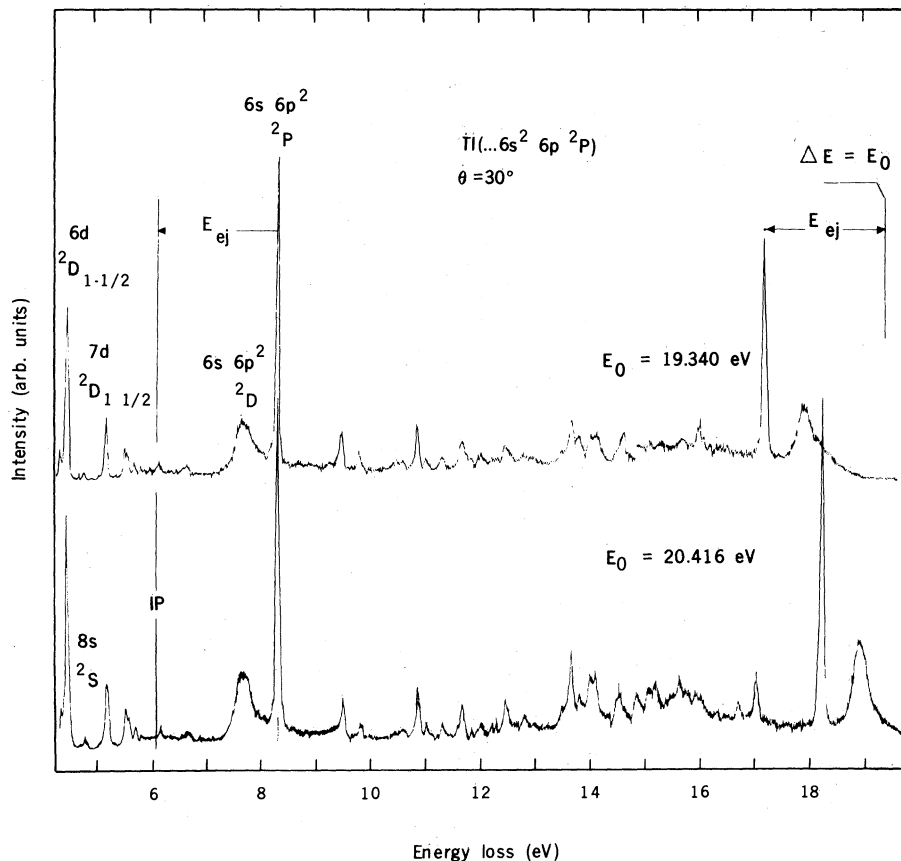


Fig. 8. Energy-loss spectrum of Tl above the first ionization limit.

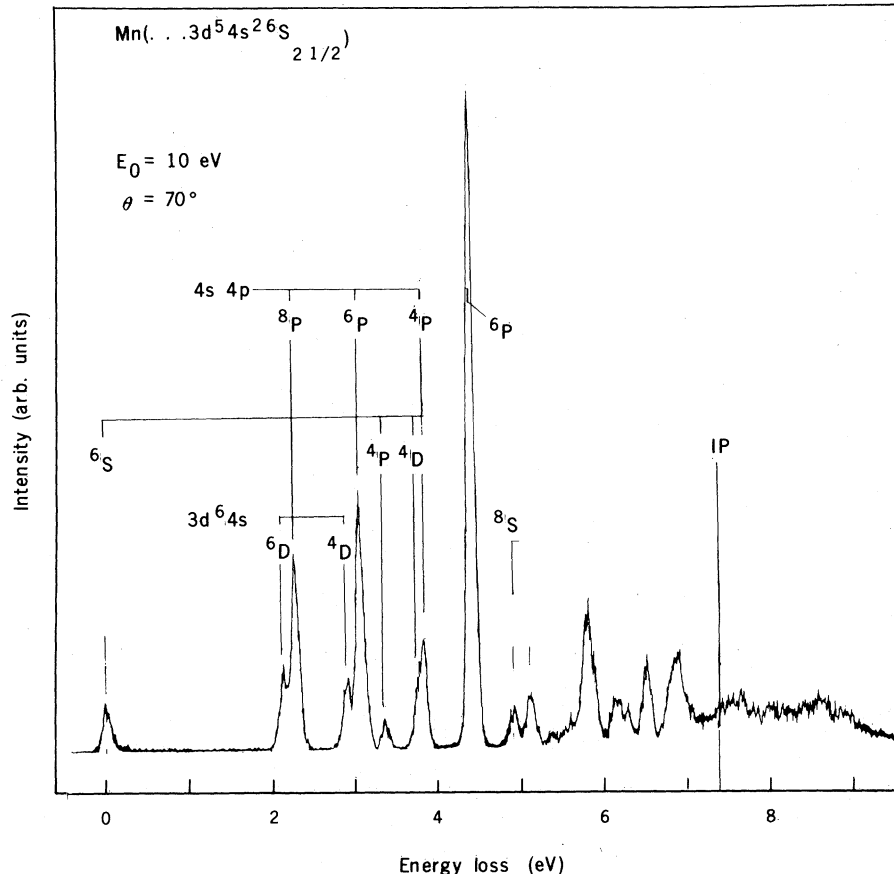


Fig. 9. Energy-loss spectrum of Mn.

been carried out. These aspects of high-energy electron scattering have been summarized by Bonham and Fink (14).

At high impact energies electrons behave like photons in excitation processes, and they can be utilized as pseudo-photons to generate photoabsorption, photoionization cross sections, and optical spectroscopic information in general. The sharp (in time) electric field experienced by the target in high-energy electron scattering may be Fourier-transformed to represent a wide range of frequencies. The electron therefore corresponds to an ideal continuum light source.

Although different optical techniques are required in different spectral regions, the electron impact spectrum can be generated by the same method in a single scan from the infrared to the x-ray region. In addition, at very short wavelengths (the far-ultraviolet and x-ray regions), the electron impact spectrum has higher resolution and higher intensity than optical spectra. Synchrotron radiation, which has come into use recently for optical absorption studies, is continuously tunable from the visible to the x-ray region, but it requires a very substantial financial investment compared to the electron impact apparatus.

The basis for the equivalence of photon and high-energy electron excitation can be understood in terms of the generalized oscillator strength. The concept of generalized oscillator strength for electron scattering was introduced by Bethe (15) and discussed in detail recently by Inokuti (16). It is defined as

$$f_{on}^G(K) = \frac{\Delta E}{2} \frac{k_0}{k_n} K^2 \frac{d\sigma_n^B}{d\Omega}(K) \quad (6)$$

where $d\sigma_n^B(K)/d\Omega$ is the Born differential cross section for process n , and K is the magnitude of the momentum transfer ($\mathbf{K} = \mathbf{k}_n - \mathbf{k}_0$). The cross section is proportional to the square of the transition matrix element, which, in the Born approximation, is given as

$$\frac{d\sigma_n^B}{d\Omega}(K) \propto |\langle \psi_n | e^{i\mathbf{K} \cdot \mathbf{r}} | \psi_0 \rangle|^2 \quad (7)$$

By expanding the exponential term in Eq. 7 in a power series and substituting this into Eq. 6, it is easy to show that at small momentum transfer (high impact energy, low scattering angle)

$$f_n^G(K) \xrightarrow{K \rightarrow 0} f_n^0 \quad (8)$$

That is, the generalized oscillator strength approaches the optical f -value f_n^0 in the limit of zero momentum transfer. Lassette *et al.* (17) extended the use of Eq. 6 to cases where the Born approx-

imation does not hold and introduced the "apparent generalized oscillator strength." They showed that this quantity also goes to the optical f -value in the limit of zero momentum transfer. This limit theorem can also be defined differently by stating that as $K \rightarrow 0$, optical selection rules apply to electron impact excitations.

Electron Impact Processes at Intermediate Energies

The area of intermediate-energy electron scattering is very important from a practical point of view. Many processes (elastic scattering, excitation, ionization, dissociation, and so on) have maximum cross sections in this energy range. Theoretical methods that are quite reliable at high and low impact energies fail in the intermediate-energy region. One has to rely on experiments both to generate information and to aid in theoretical developments. Here I demonstrate the utilization of electron scattering techniques through a few specific examples.

Electron impact excitation of metal atoms. Electron-heavy metal atom scattering is ideally suited for demonstrating a variety of electron collision processes (18). In Figs. 7 and 8 (19) the energy-loss spectrum of Tl is shown at an impact energy of 20 eV and a scattering angle of 10° . Under these conditions elastic scattering dominates. The fine-structure splitting in the ground state is easily resolved. The most prominent features correspond to the optically allowed $p \rightarrow s$ and $p \rightarrow d$ excitations. Discrete features are observed above the ionization potential corresponding to excitation of the intermediate shell ($6s$) electron, excitation of other deeper shell electrons, or simultaneous excitation of two or more electrons. The overlap of the ionization continuum with these autoionizing excited levels produces an interference phenomenon that leads to autoionization and to a resonance line shape for the excitation feature. The cross sections associated with these autoionization features are generally large and account for a substantial fraction of the overall ionization in the case of heavy elements.

In Fig. 8, which shows the part of the energy-loss spectrum above the ionization limit, the secondary (ejected) electrons are also present. They are represented by features that are mirror images of the primary electron features. For example, the $(6s6p^2) {}^2P$ state is excited at 8.3 eV, decays by autoionization to a ground-state ion (6.1 eV), and ejects a

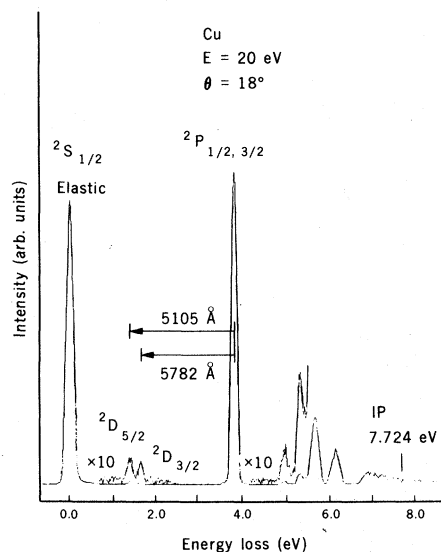
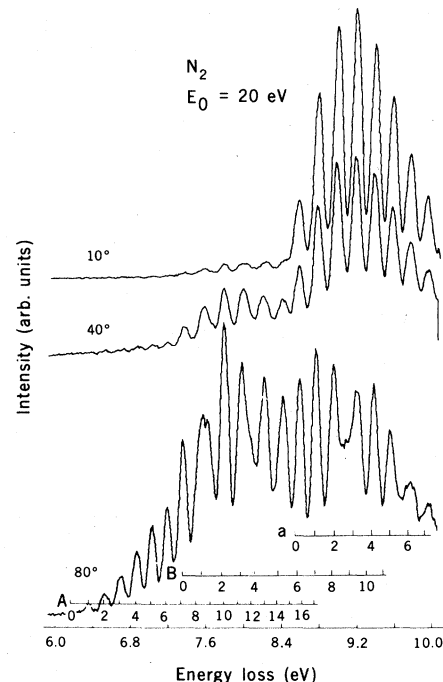


Fig. 10 (left). Energy-loss spectrum of Cu. Fig. 11 (right). Energy-loss spectra of N_2 . Vibrational structures for some of the low-lying electronic states are indicated.

secondary electron with a kinetic energy of 2.2 eV. This electron is viewed by the detector as one that has lost $E_0 - E_R = 19.3 - 2.2 = 17.1$ eV during the collision and appears at the proper energy loss, 17.1 eV, in the spectrum (upper curve in Fig. 8). It is easy to distinguish the primary scattered electron from the ejected electron by slightly changing the impact energy (to 20.416 eV in Fig. 8). The feature corresponding to excitation (and to the primary scattered electron) will remain at the same position, but the ejected electron (which still has the same residual kinetic energy) will appear at a higher energy-loss value.

An energy-loss spectrum of Mn obtained under nonoptical conditions (low impact energy, high scattering angle) is shown in Fig. 9 (20). It is interesting to note that the probability (peak height) for a number of excitation processes is higher than that for elastic scattering, and in addition to the optically allowed sextet-sextet transitions, sextet-quartet and sextet-octet spin-forbidden transitions are prominently present.

A practical use of cross-section data is illustrated in Fig. 10. Metal vapors, in general, have been considered to be efficient high-power laser media. The low-lying intermediate state can be utilized as the lower laser level in a three-level laser system, and most of the excitation energy is gained back during the lasing. However, another important factor in determining the efficiency of a laser is the efficiency of populating the upper laser level with respect to the lower laser level by electron impact; one therefore needs to know the values of the corresponding ex-



citation cross sections. This information was obtained from spectra like the one in Fig. 10, and it was concluded that, as far as cross sections were concerned, Cu was an excellent laser medium: the upper-state cross sections are large and the lower-state cross sections small (21). A similar study of Bi demonstrated that the excitation cross section for the few lowest states of Bi have comparable cross sections and efficient population inversion among them by electron impact cannot be expected (22).

Electron impact excitation of molecules. In the case of molecular targets, additional complications due to rotational-vibrational structure appear. Excitation of these degrees of freedom without electronic excitation is important at low impact energies, as discussed above, but they appear as additional structure in electronic excitations at every energy. As an example I will discuss N_2 .

Nitrogen is the most widely studied molecule from the point of view of the electron impact cross section. A large body of elastic scattering, vibrational excitation, electronic excitation, and ionization cross-section data is available for this molecule. Low-resolution spectra in Fig. 11 show the drastic influence of the scattering angle (23). At 10° the spectrum is very similar to an optical absorption spectrum with the Lyman-Birge-Hopfield system dominating. As the scattering angle is increased the character of the spectrum changes, and at high angles the spin-forbidden $A^3\Sigma$ and $B^3\Pi$ excitations appear. This effect has been widely utilized to reveal various forbidden transitions in molecules (1).

At higher energy resolution, a large number of electronic transitions and their overlapping vibrational structures have been recognized and analyzed to yield cross sections (24). A two-dimensional differential cross-section array showing the energy and angular depen-

dence for the $a^1\Pi_g$ excitation is given in Fig. 12.

A large number of electron impact excitation studies of polyatomic molecules have also been carried out by Doering and co-workers (25) and Kuppermann and co-workers (26) at low and inter-

mediate energies. Their purpose was to find and identify low-lying metastable states and to reveal general trends in the excited state energy level schemes of complex molecules. High-energy electron impact studies have also been utilized to generate photoabsorption cross sections extending into the vacuum ultraviolet region for a number of molecular species. This method has been applied to the stratospherically important halocarbons $CFCl_3$ and CF_2Cl_2 by Huebner *et al.* (27).

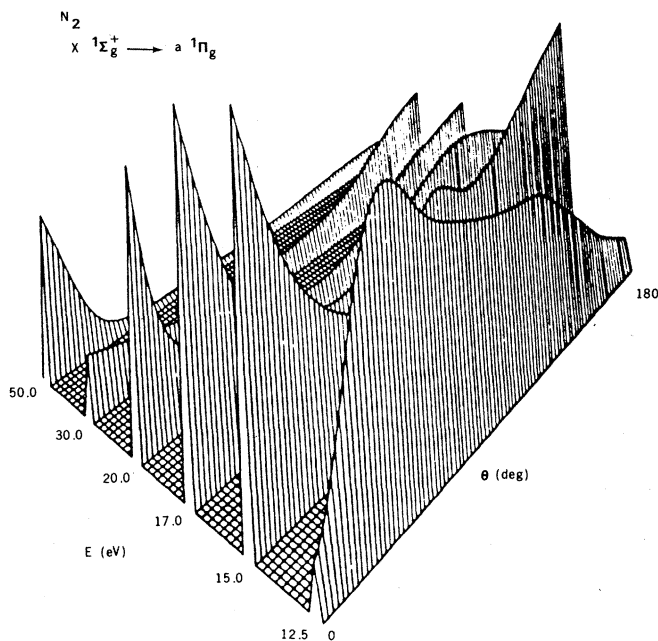


Fig. 12. Two-dimensional array of differential excitation cross sections for the $a^1\Pi_g$ state of N_2 .

Coincidence Measurements

In recent years a number of studies have been carried out in which the scattered electron is detected in coincidence with some other secondary particle (photons, electrons, ions). These measurements provide much more detailed information about the scattering process and yield quantities that cannot be obtained by conventional electron scattering techniques.

Electron-electron coincidence measurements can be interpreted in terms of differential ionization cross sections and yield information concerning electron correlation (28). At high energies one can also extract information about the structure and momentum distribution of the target from these measurements (29). Electron-photon coincidence studies have yielded radiative lifetimes (30) and scattering amplitudes (or density matrix elements) for electron impact excitation of magnetic sublevels (31). The electron-ion coincidence experiment is analogous to photoionization mass spectrometry, as demonstrated by Van der Wiel and Wiebes (32). It is not possible to discuss these studies in any more detail here.

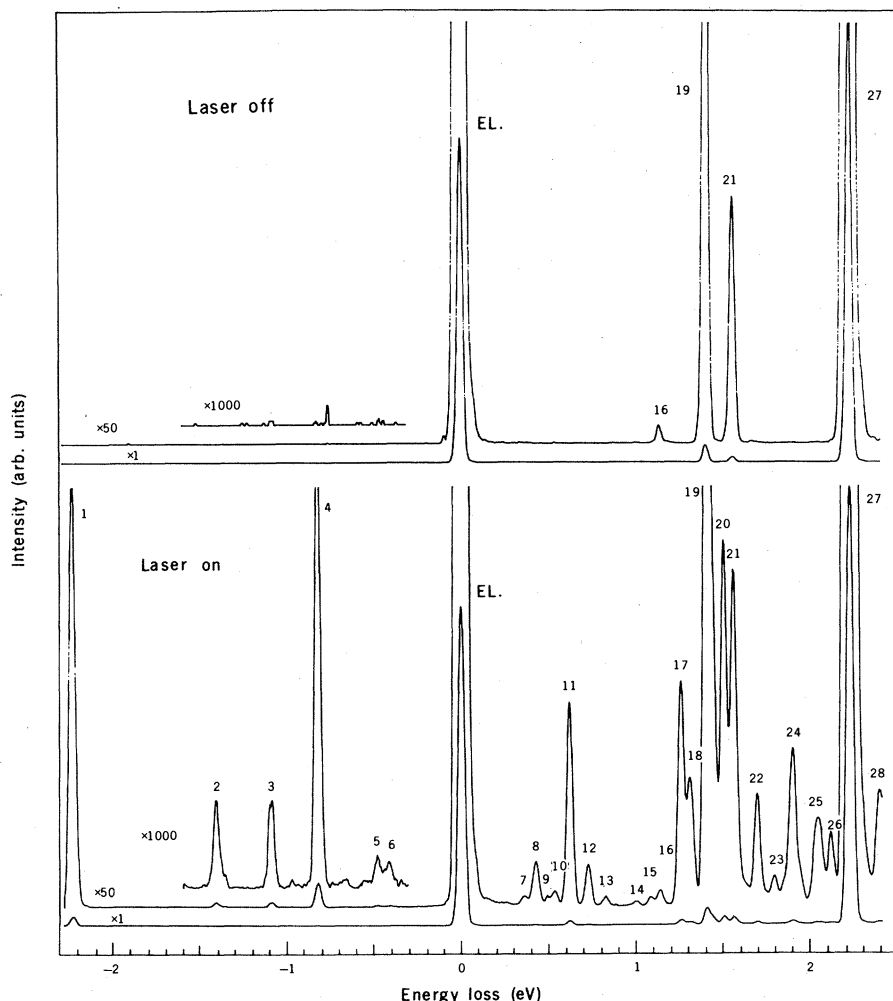


Fig. 13. Energy-loss spectrum of Ba with laser excitation off and on.

Electron-Atom Scattering in Laser Fields

With the development of tunable dye and high-power lasers, it has become feasible to carry out electron collision studies that give new kinds of information on the interaction of electron, atom, and photon. These investigations help to develop appropriate theories and are of practical importance in the field of laser plasma interactions.

A general theoretical treatment of electron scattering in a laser field is very difficult. Even electron scattering by an N -electron atom is a problem to handle, and with the addition of the photon field a number of further complications arise: (i) the energy states of the atom may be modified (dressed states), (ii) multiphoton excitation and ionization of the

atom may take place, (iii) multiphoton free electron-free electron transitions (bremsstrahlung, inverse bremsstrahlung) can occur, and (iv) the close dynamics of the scattering process can be affected by n -photon transitions in the $(N + 1)$ -electron negative atom system. The theoretical treatment of these complex processes has been limited to special situations where one particular interaction dominates and the others can be neglected or treated as perturbations.

Experimental investigations in this area have been initiated only very recently and can be divided into two categories: (i) electron scattering by laser-excited species and (ii) free-free radiative transitions.

In the first category, tunable (low-power) dye lasers are utilized to excite the target atom and scattering by the excited species is studied. Here the interaction of the electromagnetic field with the target dominates and its interaction with the free electron can be neglected. Register *et al.* (33) excited the $(6p) ^1P$ state of Ba with a wide-band laser (isotope and hyperfine levels unresolved) in a dense Ba beam (where multiple absorption and reemission cause all degenerate magnetic sublevels to be evenly populated). Electron scattering was then observed by the 1P Ba as well as cascade-populated 3P , 1D , and 3D Ba. Energy-loss spectra with the laser off and on are shown in Fig. 13. With the laser on, additional features are observed corresponding to superelastic scattering and to transitions from excited state to excited state. From this and similar spectra cross sections (averaged over isotope, hyperfine, and magnetic sublevels) were determined.

When a single-frequency dye laser is used, the energy resolution (10^{-8} eV) is good enough to selectively pump an individual hyperfine level of a specific isotope, and by selecting the proper polarization of the laser light the population of the magnetic sublevels can be controlled. In other words, a polarized target (aligned or oriented) can be prepared for electron scattering. These types of experiments make it possible to study electron scattering with an energy resolution of 10^{-8} eV and nuclear spin effects, and they yield scattering amplitudes for individual magnetic sublevel excitations. The excitation with polarized light and subsequent measurement of the superelastic electron scattering is equivalent to the time inverse electron-photon coincidence measurement (34).

Experiments in the second category have been concerned with free-free radiative transitions in strong electromagnetic fields. Here the photon energy is cho-

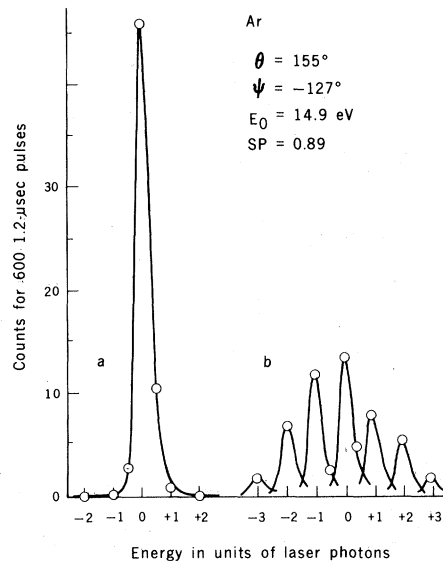


Fig. 14. Elastic scattering by Ar (a) without and (b) with a high-intensity CO₂ laser field.

sen to be far from resonance (even for multiphoton processes) and the major interaction occurs between the photon field and the free electron. The present situation in this area has been summarized by Gavrilu and Van der Wiel (35). Because of emission or absorption of photons by the scattering "free" electron (induced and inverse bremsstrahlung), the elastic (and inelastic) features appearing in energy-loss spectra have side lobes on both sides separated by an energy corresponding to the photon energy. Elastic scattering in a high-power pulsed CO₂ laser field has been studied by Weingartshofer *et al.* (36); an energy-loss spectrum for the laser off and laser on cases is shown in Fig. 14, a and b, respectively. The symbols θ , ψ , and E_0 in Fig. 14 refer to the electron scattering angle, the laser beam angle, and the electron impact energy, respectively. Here $SP = \epsilon \mathbf{k} / 2k_0$, where ϵ is the laser beam polarization vector, \mathbf{k} is the momentum transfer vector, and k_0 is the initial momentum of the electron.

Interesting situations concerning resonances can develop in connection with free-free radiative transitions. Resonances occur not only when the electron kinetic energy is proper but also when the photon energy or the electron-photon combined energy is appropriate. Such situations have been studied by Langhans (37) and Langendam and Van der Wiel (38).

I hope the examples of electron-atom (molecule) collision processes discussed in this article have given the reader a prospective view of this special, but very active, area of atomic and molecular physics. The investigations in this area yield information that is pertinent to our understanding of the basic laws of phys-

ics, and at the same time they are of considerable practical value for understanding the behavior of systems where free electrons are present.

References and Notes

1. S. Trajmar, *Acc. Chem. Res.*, in press.
2. H. S. W. Massey and E. H. S. Burhop, *Electronic and Ionic Impact Phenomena* (Clarendon, Oxford, 1969), vol. 1; H. S. W. Massey, *ibid.*, vol. 2.
3. S. Trajmar and A. Chutjian, unpublished results.
4. S. Trajmar and R. I. Hall, unpublished results.
5. S. F. Wong and G. J. Schulz, unpublished results; G. F. Schulz, in *Principles of Laser Plasmas*, G. Bekefy, Ed. (Wiley, New York, 1976), chap. 2.
6. D. F. Register, S. Trajmar, S. K. Srivastava, *Phys. Rev.*, in press.
7. S. K. Srivastava, A. Chutjian, S. Trajmar, *J. Chem. Phys.* **63**, 2659 (1975).
8. G. J. Schulz, *Phys. Rev. Lett.* **10**, 104 (1963).
9. For recent reviews see G. J. Schulz, *Rev. Mod. Phys.* **45**, 378 (1973); *ibid.*, p. 423; D. E. Golden, *Adv. At. Mol. Phys.* **14**, 1 (1978).
10. V. Fano, *Phys. Rev.* **124**, 1866 (1961); and J. W. Cooper, *Phys. Rev. A* **137**, 1364 (1965).
11. P. J. Chantry, in *Electronic and Atomic Collisions*, G. Watel, Ed. (North-Holland, Amsterdam, 1978), pp. 23-24.
12. S. Trajmar and R. I. Hall, *J. Phys. B* **7**, L458 (1974).
13. R. I. Hall, in *Electronic and Atomic Collisions*, G. Watel, Ed. (North-Holland, Amsterdam, 1978), pp. 25-41.
14. R. A. Bonham and M. Fink, *High-Energy Electron Scattering* (Van Nostrand Reinhold, New York, 1974); R. A. Bonham, in *Electron Spectroscopy: Theory, Techniques and Applications*, C. R. Brundle and A. D. Baker, Eds. (Academic Press, London, 1979), pp. 127-187.
15. H. A. Bethe, *Ann. Phys.* **5**, 325 (1930).
16. M. Inokuti, *Rev. Mod. Phys.* **43**, 297 (1971).
17. E. N. Lassette, A. Skerbele, M. A. Dillon, *J. Chem. Phys.* **50**, 1829 (1969).
18. S. Trajmar, in *Electronic and Atomic Collisions*, G. Watel, Ed. (North-Holland, Amsterdam, 1978), pp. 113-128.
19. L. S. Vuskovic, S. K. Srivastava, S. Trajmar, D. Bozinnis, *Cienc. Cult. (São Paulo)* **31**, 1018 (1979).
20. W. Williams, J. C. Cheeseborough, III, S. Trajmar, *J. Phys. B* **11**, 2031 (1978).
21. S. Trajmar, W. Williams, S. K. Srivastava, *ibid.* **10**, 3323 (1977).
22. W. Williams, S. Trajmar, D. G. Bozinnis, *ibid.* **8**, L96 (1975).
23. S. Trajmar and W. Williams, unpublished results.
24. D. C. Cartwright, *et al.*, *Phys. Rev. A* **16**, 1013 (1977); *ibid.*, p. 1041; *ibid.*, p. 1052.
25. See, for example, J. P. Doering and J. H. Moore, Jr., *J. Chem. Phys.* **56**, 2176 (1972); J. P. Doering, *ibid.* **71**, 20 (1979).
26. See, for example, W. M. Flicker, O. A. Mosher, A. Kuppermann, *ibid.* **70**, 1986 (1979); *ibid.*, p. 2003.
27. R. H. Huebner, D. L. Bushnell, Jr., R. J. Cellotta, S. R. Mielczarek, C. E. Kuyatt, *Nature (London)* **257**, 376 (1975).
28. H. Ehrhardt, K. H. Hasselbacher, K. Jung, K. Willman, *Case Stud. At. Phys.* **2**, 161 (1972).
29. I. E. McCarthy and E. Weigold, *Phys. Lett. C* **27**, 276 (1976).
30. R. E. Imhof and F. W. Read, *J. Phys. B* **4**, 450 (1971).
31. K. Blum and H. Kleinpoppen, *Phys. Rep.* **4**, 203 (1979).
32. M. J. Van der Wiel and G. Wiebes, *Physica (Utrecht)* **54**, 411 (1971).
33. D. R. Register, S. Trajmar, S. W. Jensen, R. T. Poe, *Phys. Rev. Lett.* **41**, 749 (1978).
34. I. V. Hertel and W. Stoll, *Adv. At. Mol. Phys.* **13**, 113 (1977).
35. M. Gavrilu and M. Van der Wiel, *Comments At. Mol. Phys.* **8**, 1 (1978).
36. A. Weingartshofer, E. M. Clarke, J. K. Holmes, C. Jung, *Phys. Rev. A* **19**, 2371 (1979). I am grateful to these authors for supplying a preprint of their paper and for permission to use their data in Fig. 14.
37. L. Langhans, *J. Phys. B* **11**, 2361 (1978).
38. P. J. K. Langendam and M. J. Van der Wiel, *ibid.*, p. 3603.
39. I wish to thank my collaborators whose work has been cited. This article represents the results of one phase of research conducted at the Jet Propulsion Laboratory under NASA contract NAS 7-100.